

ORIGINAL ARTICLE

TASP1 mutation in a female with craniofacial anomalies, anterior segment dysgenesis, congenital immunodeficiency and macrocytic anemia

Daniel M. Balkin^{1,2}  | Menitha Poranki³ | Craig M. Forester⁴ | Morna J. Dorsey⁴ | Anne Slavotinek³ | Jason H. Pomerantz^{1,2,5}

¹Division of Plastic and Reconstructive Surgery, Department of Surgery, University of California San Francisco, San Francisco, California

²Craniofacial Center, University of California San Francisco, San Francisco, California

³Division of Genetics, Department of Pediatrics, University of California San Francisco, San Francisco, California

⁴Division of Pediatric Allergy, Immunology & Bone Marrow Transplantation, Department of Pediatrics, University of California San Francisco, San Francisco, California

⁵Department of Orofacial Sciences, University of California San Francisco, San Francisco, California

Correspondence

Jason H. Pomerantz, Division of Plastic and Reconstructive Surgery, Department of Surgery, University of California San Francisco, 400 Parnassus Avenue, San Francisco, CA 94143.

Email: jason.pomerantz@ucsf.edu

Abstract

Background: Threonine Aspartase 1 (Taspase 1) is a highly conserved site-specific protease whose substrates are broad-acting nuclear transcription factors that govern diverse biological programs, such as organogenesis, oncogenesis, and tumor progression. To date, no single base pair mutations in Taspase 1 have been implicated in human disease.

Methods: A female infant with a new pattern of diagnostic abnormalities was identified, including severe craniofacial anomalies, anterior and posterior segment dysgenesis, immunodeficiency, and macrocytic anemia. Trio-based whole exome sequencing was performed to identify disease-causing variants.

Results: Whole exome sequencing revealed a normal female karyotype (46,XX) without increased regions of homozygosity. The proband was heterozygous for a de novo missense variant, c.1027G>A predicting p.(Val343Met), in the *TASP1* gene (NM_017714.2). This variant has not been observed in population databases and is predicted to be deleterious.

Conclusion: One human patient has been reported previously with a large *TASP1* deletion and substantial evidence exists regarding the role of several known Taspase 1 substrates in human craniofacial and hematopoietic disorders. Moreover, Taspase 1 deficiency in mice results in craniofacial, ophthalmological and structural brain defects. Taken together, there exists substantial evidence to conclude that the *TASP1* variant, p.(Val343Met), is pathogenic in this patient.

KEYWORDS

anterior segment dysgenesis, congenital immunodeficiency, craniofacial anomaly, macrocytic anemia, Taspase 1

1 | CLINICAL DESCRIPTION

The female patient was born to healthy parents of Caucasian and Asian ethnicities without a significant family history or known consanguinity. The pregnancy was complicated by maternal diabetes mellitus treated by oral sulfonylurea therapy. Prenatal sonograms were normal. The patient was born at 38 + 1 weeks of gestation by spontaneous vaginal delivery to a 34-year-old G2P0-1 mother. The baby weighed 2,540 grams (3–10th percentile) with APGAR scores of 3, 7, and 7 at 1, 5, and 10 min respectively. She required continuous positive airway pressure and intubation for respiratory distress. Several craniofacial dysmorphic features were noted shortly after birth, including a large anterior fontanelle, brachycephaly, sparse scalp hair, a flat facial profile with flat nasal bridge, prominent epicanthic folds, midface hypoplasia, cupped ears with dysplastic helices without pits or tags, and a high arched palate (Figure 1a–c). Large congenital hemangiomas of the ears and oral commissure were noted (Figure 1a). Eyelid ptosis and corneal clouding (Figure 1b) prompted ophthalmologic examination at 3 days of age, which revealed bilateral anterior segment dysgenesis and elevated intraocular pressures of 40–45 mm Hg resulting in a diagnosis of glaucoma.

Magnetic resonance imaging (MRI) at 3 days of age demonstrated multifocal ischemia of the brain parenchyma, primarily involving the left temporal lobe with an associated extra-axial hemorrhagic collection and with areas of microhemorrhage, likely reflective of embolic etiology. Anomalous course of the bilateral optic nerves was noted. The optic globes were prominent and oblong in appearance compatible with known congenital glaucoma and coloboma. Delayed sulcation of the brain was noted and a brachycephalic and slightly cloverleaf head shape were noted (Figure 2a–c). Follow-up MRI demonstrated thinning of the corpus callosum and ventriculomegaly. (Figure 2d).

The patient's progress was complicated by her complex medical needs. Laryngoscopy revealed moderate pharyngolaryngomalacia with mild tracheomalacia. Swallow evaluation demonstrated oropharyngeal dysfunction prompting gastrostomy tube placement at 2 months of age. The patient was diagnosed with an atrial septal defect versus patent foramen ovale, which closed spontaneously. Bilateral hip dislocations were managed by bracing. Audiology assessment noted conductive hearing loss secondary to diminutive ear canals that was aided by placement of a bone-anchored hearing aid at 1 year of age.

The patient's newborn screen was abnormal for severe combined immunodeficiency given low T-cell receptor excision circles. Follow-up testing demonstrated T cell lymphopenia, complete absence of B cells, reduced NK cells and low levels of IgA and IgM. Her agammaglobulinemia was treated with monthly intravenous immunoglobulin administration

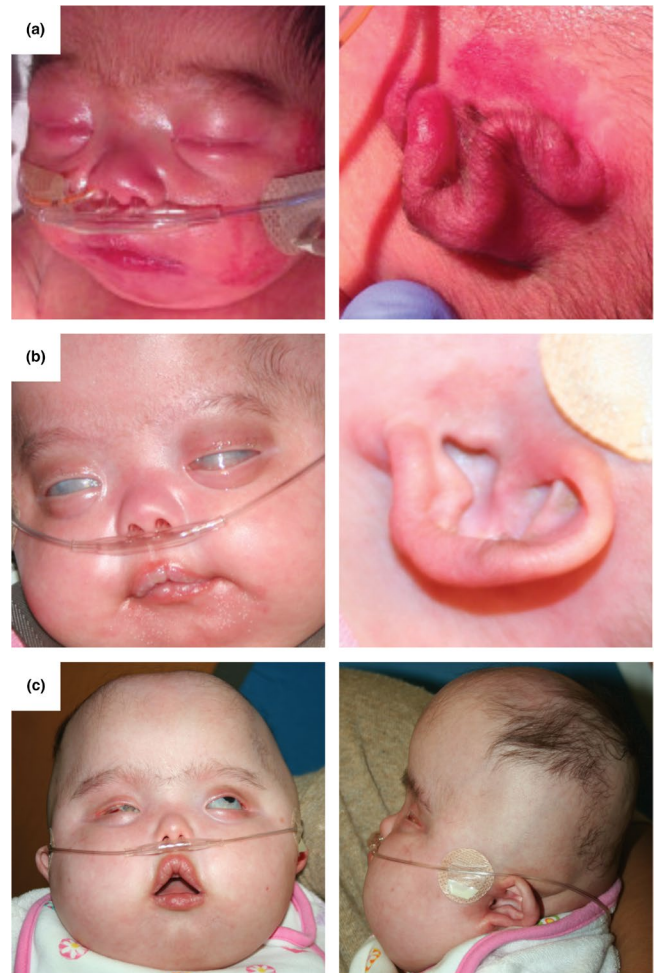


FIGURE 1 Clinical photographs of a female patient with a de novo missense variant in the *TASPI* gene. Frontal (left) and lateral (right) views at 2 days (a), 2 months, note involution of the congenital hemangioma (b) and 17 months of age (c)

until 3 years of age. The patient required monthly packed red blood cell transfusions for diminished hemoglobin. Imaging and laboratory testing was negative for immune-mediated destruction or acute losses in urine or stool. For concern of an inherited marrow failure syndrome, diepoxybutane-induced chromosome breakage and telomere analyses were performed, which were unremarkable. Hemoglobin electrophoresis did not reveal elevated fetal hemoglobin and red blood cell erythrocyte adenosine deaminase levels were normal. Imaging was negative for thymic mass and the patient had no lymphadenopathy or organomegaly. Bone marrow evaluation demonstrated normal cellularity, trilineage hematopoiesis and appropriate maturation of all phases of erythropoiesis. The patient's transfusion dependency lessened but anemia persisted with insufficient reticulocytosis, while the mean corpuscular volume and erythropoietin levels steadily rose. Given the patient's pronounced macrocytosis and poor reticulocytosis, repeat bone marrow evaluation was performed, which revealed a paucity of early erythroid precursors without micromegakaryopoiesis,

low level hemophagocytosis and no abnormalities in lymphopoiesis or granulocytic maturation. Subsequently, the patient has been closely followed with a stable mild thrombocytopenia and macrocytic anemia. Collectively, the patient's hematological presentation is most consistent with a red cell aplasia in the setting of congenital immunodeficiency.

Computed tomography (CT) scans were obtained at two and 14 months-of-age to assess the craniofacial skeleton, which revealed dysmorphism of the skull base, patency of the major craniofacial sutures and generalized hypo-ossification of the cranial vault (Figure 2e–g). Hypo-ossification primarily affected the skull base (Figure 2f), including complete failure of ossification of the bilateral temporal squamosa (Figure 2e,g) and greater wing of the sphenoid bones (Figure 2e, triangle). Bilateral auditory canal stenosis was present. A small foramen magnum (Figure 2d) and large anterior fontanelle (Figure 2g) were associated with hydrocephalus but absence of a Chiari malformation (Figure 2d).

Optic pathway defects included an anomalous course of the bilateral optic nerves and severe bilateral anterior segment dysgenesis, congenital glaucoma, and retinal detachment as seen on prior MRI.

Clinical management of the craniofacial defects was complex. Persistent hypo-ossification of the cranial vault and progressive herniation of intracranial contents prompted vault reconstruction, which was performed at 17-months of age (Figure 2h). The temporal lobes were reduced into the cranial cavity and protected with sliding interdigitating parietal bone grafts. A bandeau frontal orbital advancement was performed to protect the globes and minimize the brachycephalic form, and the anterior fontanelle was partially reduced with frontal and parietal bone grafts. Demineralized bone matrix was applied to encourage ossification of the remaining defects. The degree of midface hypoplasia was insufficient to warrant early midface advancement. Upper airway obstruction and central

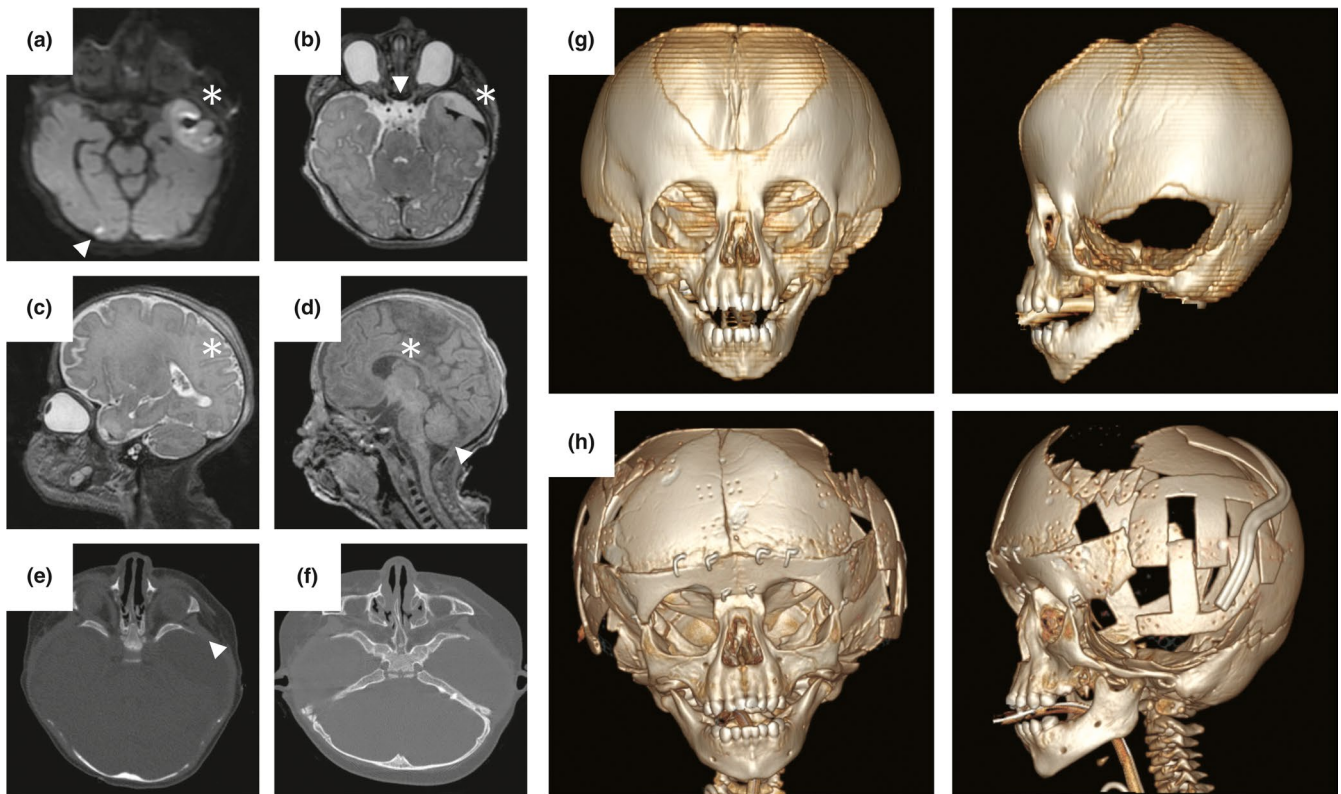


FIGURE 2 Pre- and postoperative cross-sectional imaging. Magnetic resonance imaging at 3 days of age (a–d). Axial diffusion-weighted image revealing multifocal ischemia involving the left temporal lobe (star) with additional areas of microhemorrhage (triangle) (a). Axial multiplanar reconstruction illustrating left temporal lobe extra-axial hemorrhagic collection (star) and anomalous course of the bilateral optic nerves (triangle) (b). Axial multiplanar reconstruction (b) and sagittal T2-weighted (c) images with notable prominent and oblong optic globes, as well as delayed parenchymal sulcation (c, star). Sagittal T1-weighted image demonstrating thinning of the corpus callosum (star) and absence of a Chiari malformation (triangle) (d). Pre-operative computed tomography at 14-months of age (e–g). Axial image revealing complete failure of ossification of the greater wing of the sphenoid bones (triangle) and bilateral temporal squamosa (e). Axial image demonstrating hypo-ossification of the skull base (f). Three dimensional reconstruction with large anterior fontanelle (frontal, left) and absence of temporal bone squamosa (lateral, right). Postoperative computed tomography three dimensional reconstruction at 17-months of age demonstrating sliding interdigitating parietal bone grafts (lateral, right) and a bandeau orbital advancement with partial reduction of the anterior fontanelle with frontal and temporal bone grafts (frontal, left) (h)

apnea were treated with tonsillectomy and adenoidectomy, as well as supplemental oxygen respectively. Posterior fossa crowding improved based on serial cross sectional imaging. The patient's ocular anomalies were treated with bilateral corneal transplantation and tube shunting for glaucoma, as well as repair of right-sided retinal detachment.

At 2 years of age, the patient was able to recognize her parents and reach toward objects. She was able to sit up from a supine position and ride a bike with training wheels. At 3 years of age, the patient's height was 85 cm (first percentile), weight was 10.6 kg (less than first percentile), and occipito-frontal circumference was 52 cm (90-97th percentile). She had persistent marked scalp alopecia. Her eyebrows were sparse and her eyelashes were absent. Craniofacial dysmorphic features persisted as noted at birth. Her nipples were wide-spaced. Her hands and feet were small, with pointed upper extremity digits and small thin-appearing nails. The left palm measured 5.8 cm (3–25th percentile) and the third finger measured 3 cm (less than third percentile). The skin of her feet was reddened and clinodactyly of the fourth and fifth toes was notable. The patient had mildly reduced tone without focal neurological signs.

Additional investigations included a skin biopsy that was negative for alopecia areata despite the absence of scalp hair. In addition, a whole genome comparative genomic hybridization (CGH) array (using a custom 180K oligonucleotide array) did not reveal any pathogenic copy number variants (arr(1–22,X)x2).

2 | METHODS

2.1 | Whole exome sequencing

Whole exome sequencing (WES) with blood-derived DNA from the proband and both biological parents was performed as a clinical test in 2014 (University of California, Los Angeles) according to published methods (Lee et al., 2014). Re-analysis was performed in 2016 according to the same methodology. In brief, extracted DNA was subjected to exome sequencing using the Agilent Technologies

SureSelect Human All Exon 50 Mb XT kit with an Illumina HiSeq 2500 (Illumina). Sequencing data were aligned to both the human reference and mitochondrial genomes, and then variants were annotated for potential impact on protein function, allele frequency in the general population and evidence of prior disease relevance.

2.2 | Permission/approval

Written authorization was obtained for publication of this report and accompanying images. In addition, this publication adheres to the University of California San Francisco Human Research Protection Program policy and guidelines.

3 | RESULTS

Whole exome sequencing revealed a normal female karyotype (46,XX) without regions of homozygosity greater than five megabases (Mb). The proband was heterozygous for a de novo missense variant c.1027G>A, predicting p.(Val343Met), in the *TASPI* gene (NM_017714.2; OMIM 608270). This variant has not been seen in population databases and in silico prediction algorithms (SIFT, PolyPhen, CADD and MutationAssessor; Adzhubei et al., 2010; Kircher et al., 2014; Ng & Henikoff, 2001; Reva, Antipin, & Sander, 2011) suggest that this mutation is deleterious/damaging (Table 1). An additional variant c.4981G>A, predicting p.(Gly1661Ser), in the *COL4A2* gene (OMIM 120090) was inherited from the patient's healthy mother. Both sequence variants in *TASPI* and *COL4A2* were reported as variants of unknown significance and possibly related to the proband's phenotype (Table 1). There were no secondary findings. Re-analysis of sequencing in 2016 demonstrated the same two variants without a change in the report or variant interpretation. Since deleterious sequence variants in the *COL4A2* gene can cause intracranial hemorrhage, structural brain changes, anterior chamber eye defects, and optic nerve hypoplasia (Kuo, Labelle-Dumais, & Gould, 2012), a brain MRI of the proband's mother was performed, which was normal.

TABLE 1 Sequence variants identified in proband whole exome sequencing

Gene/transcript	Nucleotide	Protein	Inheritance	Zygoty	ExAC browser/1000 genomes/GnomAd	Interpretation	Human phenotype
<i>TASPI</i>	c.1027G>A	p.Val1343Met	De novo	Het.	—	VUS	Nil reported
<i>COL4A2</i>	c.4981G>A	p.Gly1661Ser	Maternal	Het.	—	VUS	<i>COL4A2</i> syndrome

Note: All sequence variants from the exome reports in 2013 and 2016 have been listed in the Table. Abbreviations: Het., heterozygous; VUS, variant of unknown significance.

4 | DISCUSSION

We present a female child with a new pattern of diagnostic abnormalities comprising craniofacial dysmorphism, congenital immunodeficiency, infantile facial hemangioma, severe optic pathway anomalies, and scalp and face alopecia (Table 2). Her growth parameters have shown height and weight less than the third percentile, and she has experienced significant delays in early milestones. WES demonstrated a de novo variant in the *TASPI* gene, p.(Val343Met), that is not present in control databases and is predicted to be deleterious.

There is only one other reported case with deleterious variants in *TASPI*. An infant with developmental delay, acquired microcephaly, distinctive facial features, and multiple congenital anomalies involving skeletal, cardiac, and renal systems was found to harbor a homozygous deletion including exons five to 10 of *TASPI* (Suleiman, Mundt, Sampath, & El-Hattab, 2018). This child had excess forehead hair, arched and thick eyebrows, synophrys, a broad nasal bridge, downslanted palpebral fissures, wide-set eyes, epicanthus, low-set ears, an overfolded right ear helix, microretrognathia, thin upper lip and downturned corners of mouth. A left-sided preauricular skin tag, webbed neck, preaxial polydactyly of the right hand and bilateral single palmar creases were also observed (Suleiman et al., 2018). Echocardiography demonstrated a small patent foramen ovale with a left to right shunt and a ventricular septal defect, while renal sonography revealed mild left-sided hydronephrosis. The clinical features in the reported child with a multi-exon *TASPI* deletion are different from our patient with the novel *TASPI* p.(Val343Met) variant. Conceivably, this could reflect different pathogenic mechanisms of disease with deletion homozygosity implying loss-of-function compared to a missense variant reflecting haploinsufficiency, gain-of-function, or a dominant-negative

effect. One additional explanation that could account for the genetic and pathologic differences between both patients is that the de novo heterozygous variant in the *TASPI* gene observed in our patient (as opposed to the previously reported homozygous deletion) occurs in the setting of a maternally inherited *COL4A2* variant, which may permit Taspase 1-mediated penetrance of the disease phenotype in the heterozygous state.

Taspase 1 encodes a highly conserved endopeptidase that uses a NH₂-terminal threonine as the active-site nucleophile to proteolyze polypeptide substrates following aspartate (Chen et al., 2012; Hsieh, Cheng, & Korsmeyer, 2003). The 50 kD Taspase 1 alpha-beta proenzyme undergoes intramolecular auto proteolysis generating the active 28 kD alpha/22 kD beta heterodimer (Figure 3a). Knockdown of Taspase 1 in HeLa cells results in the appearance of unprocessed Mixed Lineage Leukemia (*MLL*; also known as *MLL1* and *KMT2A*; OMIM 159555) protein and dysregulation of HOX gene expression (Figure 3b). Taken together, Taspase 1 substrates are broad-acting nuclear transcription factors that direct the expression of numerous target genes (Capotosti, Hsieh, & Herr, 2007; Hsieh, Cheng, et al., 2003; Takeda et al., 2006; Zhou et al., 2006).

In an effort to assess the function of Taspase 1 in vivo, Takeda et al. generated Taspase 1 deficient mice using a Cre-lox gene targeting strategy on a mixed 129SvJ/C57BL/6 genetic background to delete exon nine of the murine gene that contains the active site threonine 234 residue (Takeda et al., 2006). Although no abnormalities were observed in Taspase 1 heterozygous (\pm) mice, heterozygous incrosses revealed that Taspase 1 knockouts ($-/-$) were born without apparent respiratory distress, but exhibited early postnatal lethality with 87% of animals not surviving beyond postpartum day two. The Taspase 1 deficient pups were smaller than littermate

TABLE 2 Clinical features of patient with p.Val343Met in *TASPI*

Clinical features of patient with <i>TASPI</i> mutation	Proband	<i>TASPI</i> deficient mice
Underdevelopment of cerebral cortex	+	+
Microphthalmia	-	+
Anophthalmia	-	+
Agnathia	Oropharyngeal dysphasia pharyngolaryngomalacia, mild tracheomalacia	+
Acephaly	-	+
Decreased body size	+	+
Decreased heart size	Septal defect	+
Feeding difficulties	+	+
Skeletal abnormalities	+	+
Impaired expansion of CD4+/CD8+ double-positive thymocytes	+	+

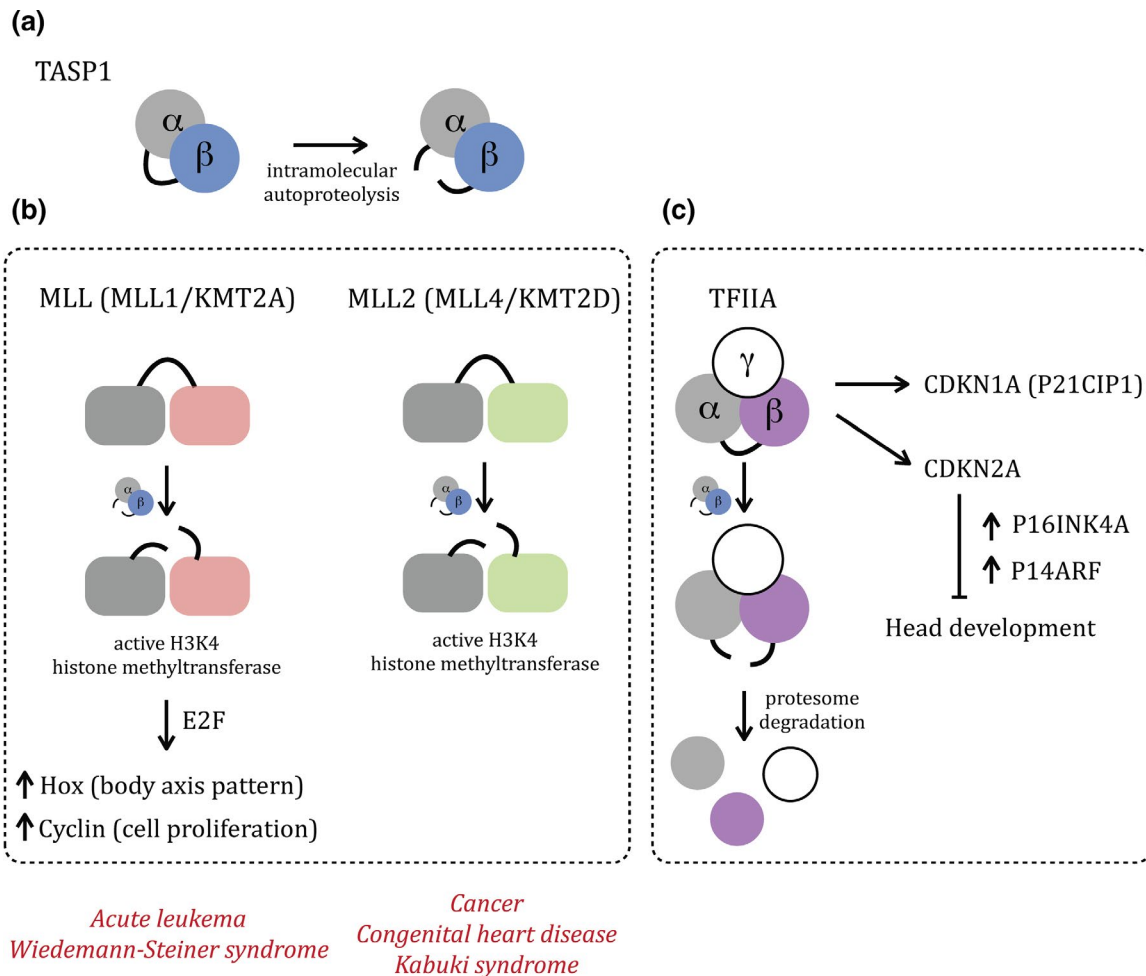


FIGURE 3 *TASP1*, downstream targets and human conditions. The 50 kD Taspase 1 alpha-beta proenzyme undergoes intramolecular auto proteolysis generating the active alpha-beta heterodimer (a). *MLL/KMT2A* is cleaved by *TASP1*, resulting in active histone H3 methylation and downstream transcriptional changes (b, left). *TASP1* also uses *MLL2/KMT2D* as substrate rendering active histone modification (b, right). The transcription factor TFIIA (*GTF2A1*), an additional *TASP1* substrate, is one of several basal transcription factors required for all transcriptional events that use RNA polymerase II. Following Taspase 1-mediated cleavage, TFIIA is susceptible to proteasome-mediated degradation (c, left). However, when *TASP1* is absent, there is an upregulated expression of TFIIA target genes (*CDKN1A/P21CIP1* and *CDKN2A/P16INK4A/P14ARF*), which impacts craniofacial development (c, right). Of note, red text indicates human pathologies resulting from mutations in the indicated genes (*TASP1*, *MLL/KMT2A*, and *MLL2/KMT2D*)

controls, and exhibited severe skeletal abnormalities, including classic homeotic transformations of the vertebrae and ribs, a shortened skull, and distorted tongue. The pups also exhibited abnormal outgrowth of cranial nerves and a reduction in hematopoietic stem cell populations and thymocytes (Takeda et al., 2006). Efforts to characterize the underlying mechanism by which Taspase 1 regulates animal size were performed in mouse embryonic fibroblasts and in the thymus, where Taspase 1 is abundantly expressed. Knockout cells exhibited impaired cell cycle progression, with dysregulated expression of several cyclin-dependent kinases together with a profound proliferation defect in the developing thymus, indicating an essential role for Taspase 1 in cell cycle regulation (Takeda et al., 2006).

The initial Taspase 1 mutant mouse exhibited a shortened skull and a distorted tongue on a mixed 129SvJ/C57BL/6 background (Takeda et al., 2006). Since the C57BL/6 background can confer a greater susceptibility to cranial malformations (Matsuo, Kuratani, Kimura, Takeda, & Aizawa, 1995; Shawlot & Behringer, 1995), the original line of Taspase 1 mutant mice were backcrossed to C57BL/6. Taspase 1 deficiency on the C57BL/6 genetic background resulted in severe craniofacial malformations, including anophthalmia, microphthalmia, agnathia, ethmocephaly, and acephaly (Table 2). Analysis at embryonic day (E)9.5-E10.5 demonstrated that the knockout embryos exhibited hypoplasia or absence of the prosencephalons, nasal processes, and first pharyngeal arches. In addition, E14.5-E18.5 knockout embryos

demonstrated severe underdevelopment or complete absence of the cerebral cortex, striatum, and lower jaw (Takeda et al., 2015).

Comparative expression microarray analyses were performed on the prosencephalons and mesencephalons of Taspase 1 wild-type and knockout E10.5 embryos to determine the mechanisms through which Taspase 1 organizes head morphogenesis (Takeda et al., 2015). Gene set enrichment analysis demonstrated a significant association between cell cycle regulators, specifically *CDKN1A* (*P21CIP1*; OMIM 116899) and *CDKN2A* (OMIM 600160), and altered cranial development. The *CDKN2A* locus encodes two distinct proteins from alternative open reading frames, namely, *P16INK4A*, a cyclin-dependent kinase inhibitor, and Alternative Reading Frame (*ARF*) that promotes p53 (*TP53*; OMIM 191170) stabilization that in turn induces cell cycle arrest or apoptosis depending on context (Pomerantz et al., 1998; Sherr, 2001). Taspase 1 knockout embryos demonstrated a two-three fold enrichment of the mRNA levels of *P16INK4A*, *ARF*, and the p53 target, *CDKN1A/P21CIP1*, at E10.5 compared to littermate controls. Interestingly, deficiency of *CDKN2A* in *TASPI/CDKN2A* compound mutant mice rescued the Taspase 1 craniofacial knockout phenotype, suggesting that *CDKN2A* functions downstream of Taspase 1 as an effector of the Taspase 1 mutant phenotype and of abnormal cell cycle regulation (Takeda et al., 2015) (Figure 3c).

Aberrant cell cycle regulation has been implicated in several other craniofacial syndromes, most notably, Treacher-Collins syndrome (Jones et al., 2008; Li et al., 2013). In patients with Treacher-Collins syndrome and in animal models of this disease, mutations in *TCOF1* (OMIM 606847) result in upregulation of p53 and its downstream effectors, similar to the pathway described for the Taspase 1 mutant mice. However, despite this shared cell cycle and apoptosis pathway, the different phenotypic features in the Taspase 1 mutant mice compared to those resulting from *TCOF1* mutations indicate that the two genes also have divergent functions.

The Taspase 1 substrates *MLL/KMT2A* and *MLL2/KMT2D* (OMIM 602113) have been implicated in human hematopoietic and craniofacial disorders. Taspase 1 was cloned as the enzyme responsible for cleavage of *MLL/KMT2A*, which encodes a 3,969-amino acid nuclear DNA-binding protein that maintains correct HOX gene expression patterns through histone H3 methylation (Hsieh, Ernst, Erdjument-Bromage, Tempst, & Korsmeyer, 2003; Milne et al., 2002; Nakamura et al., 2002). Characteristic chromosomal translocations found in human acute leukemias disrupt the *MLL/KMT2A* locus generating chimeric fusion proteins between *MLL/KMT2A* and several translocation partners (Ayton & Cleary, 2001). Gene expression profiles of infant leukemias exhibiting *MLL/KMT2A* translocations display characteristic features, which help to identify poor prognosis leukemias from others, including

disregulated HOX gene expression (Armstrong et al., 2002; Yeoh et al., 2002). In addition, mutations in *MLL/KMT2A* have been identified in patients with Wiedemann-Steiner Syndrome, which is a multi-system disorder characterized by hypertrichosis cubiti, short stature, intellectual disability, and distinctive facial features (Jones et al., 2012; Figure 3b).

MLL2/KMT2D is also a well-described Taspase 1 substrate (Takeda et al., 2006) (Figure 3b). It is a 5,537-amino acid histone H3 lysine 4 mono-methyltransferase and member of a protein family of Set1-like H3K3 methyltransferases, which also contains *MLL/KMT2A* (Lee et al., 2013). *MLL2/KMT2D* is widely expressed in adult tissues and co-localizes with lineage determination transcription factors on transcriptional enhancers. It plays an important role in cellular differentiation and embryonic development (Lee et al., 2013; Prasad et al., 1997). Moreover, it has been shown to function in cell fate transition (Lee et al., 2013; Wang et al., 2016), liver metabolism (Kim et al., 2016, 2015) as well as tumor suppression (Chen et al., 2014; Lee et al., 2009; Ortega-Molina et al., 2015). In humans, mutations in *MLL2/KMT2D* have been demonstrated in various forms of cancer (Rao & Dou, 2015). Moreover, heterozygous germline mutation in *MLL2/KMT2D* is responsible for Kabuki Syndrome, a rare autosomal dominant multisystem disorder characterized by mental retardation, short stature, hip dysplasia, skeletal abnormalities of the hands and vertebrae, congenital heart disease, and craniofacial dysmorphism. Typical facial characteristics include long palpebral fissures (with eversion of the lateral third of the lower eyelids), broad and depressed nasal tip, prominent ears and a cleft or high-arched palate (Ng et al., 2010; Niikawa, Matsuura, Fukushima, Ohsawa, & Kajii, 1981; Zaidi et al., 2013). Moreover, immune abnormalities are a frequent manifestation of Kabuki Syndrome with hypogammaglobinemia a frequent finding (Hoffman et al., 2005).

Two additional Taspase 1 substrates, a ubiquitously expressed general transcription factor (TFIIA) alpha-beta (*GTF2A1*; OMIM 600520) and the testis-enriched general transcription factor (ALF) alpha-beta (*GTF2A1L*; OMIM 605358), have not been implicated in human disease. This likely reflects an essential role for gene function in cellular viability. TFIIA alpha-beta is a 376-amino acid protein involved in RNA polymerase II-dependent transcription. It cooperates with RNA polymerase II, the TATA-box-binding protein (TBP), and other TBP-associated proteins to form a transcription pre-initiation complex on the TATA-box sequence of promoter elements upstream of transcription initiation sites (Tan, Hunziker, Sargent, & Richmond, 1996). TFIIA alpha-beta is cleaved by Taspase 1 to form TFIIA alpha and TFIIA beta (Zhou et al., 2006; Figure 3c). Since the Taspase 1 knockouts adequately support bulk transcription, TFIIA alpha-beta cleavage does not appear essential. However, Taspase 1-mediated proteolytic cleavage of TFIIA alpha-beta may impact protein turnover and therefore allow

for fine-tuning cellular levels of transcription (Hoiby, Zhou, Mitsiou, & Stunnenberg, 2007). Given that TFIIA alpha-beta serves a critical function in overall general transcription, it is not surprising that TFIIA alpha-beta deletion in *Saccharomyces cerevisiae* is lethal (Kang, Auble, Ranish, & Hahn, 1995; Ranish, Lane, & Hahn, 1992).

Taspase 1 also uses ALF alpha-beta as substrate for cleavage. ALF alpha-beta is a 478-amino acid protein that serves as a germ cell-specific TFIIA alpha-beta homolog, cooperating with RNA polymerase II and various other transcription factors to synthesize eukaryotic mRNA (Upadhyaya, Lee, & DeJong, 1999). Expression has been demonstrated in the testis of mouse tissues (Han et al., 2001). Similar to TFIIA alpha-beta, no deleterious sequence variants in ALF alpha-beta have been described in association with human disease.

We posit that there exists substantial evidence to support a causative role for *TASPI* in the pathogenesis of this child's phenotype. The c.1027G>A variant has not previously been observed in the general population and the valine amino acid residue at position 343 (*TASPI*^{V343}) is

highly conserved evolutionarily (Figure 4), with several in silico prediction algorithms (SIFT, PolyPhen, CADD, and MutationAssessor) suggesting that this mutation is deleterious and likely damaging (Adzhubei et al., 2010; Kircher et al., 2014; Ng & Henikoff, 2001; Reva et al., 2011; Table 1). Activity of Taspase 1 is dependent on the formation of a heterotetramer, thus creating the binding groove for substrates (Khan, Dunn, & Tong, 2005). Although V343 does not lie within the enzyme catalytic site, this residue sits in close proximity and across the binding groove from residue T234, which may mechanistically imply that *TASPI*^{V343M} affects substrate binding/specificity. Further investigation is underway into whether this mutation impairs autoproteolysis of Taspase 1, formation of the active heterotetrameric complex or potentially alters the specificity of the proteolytic activity toward substrate targets thus remodeling downstream transcriptional signaling. Taken together with the known function of Taspase 1 in mouse development, evidence suggests that this Taspase 1 variant is responsible for the birth defects observed in this patient.

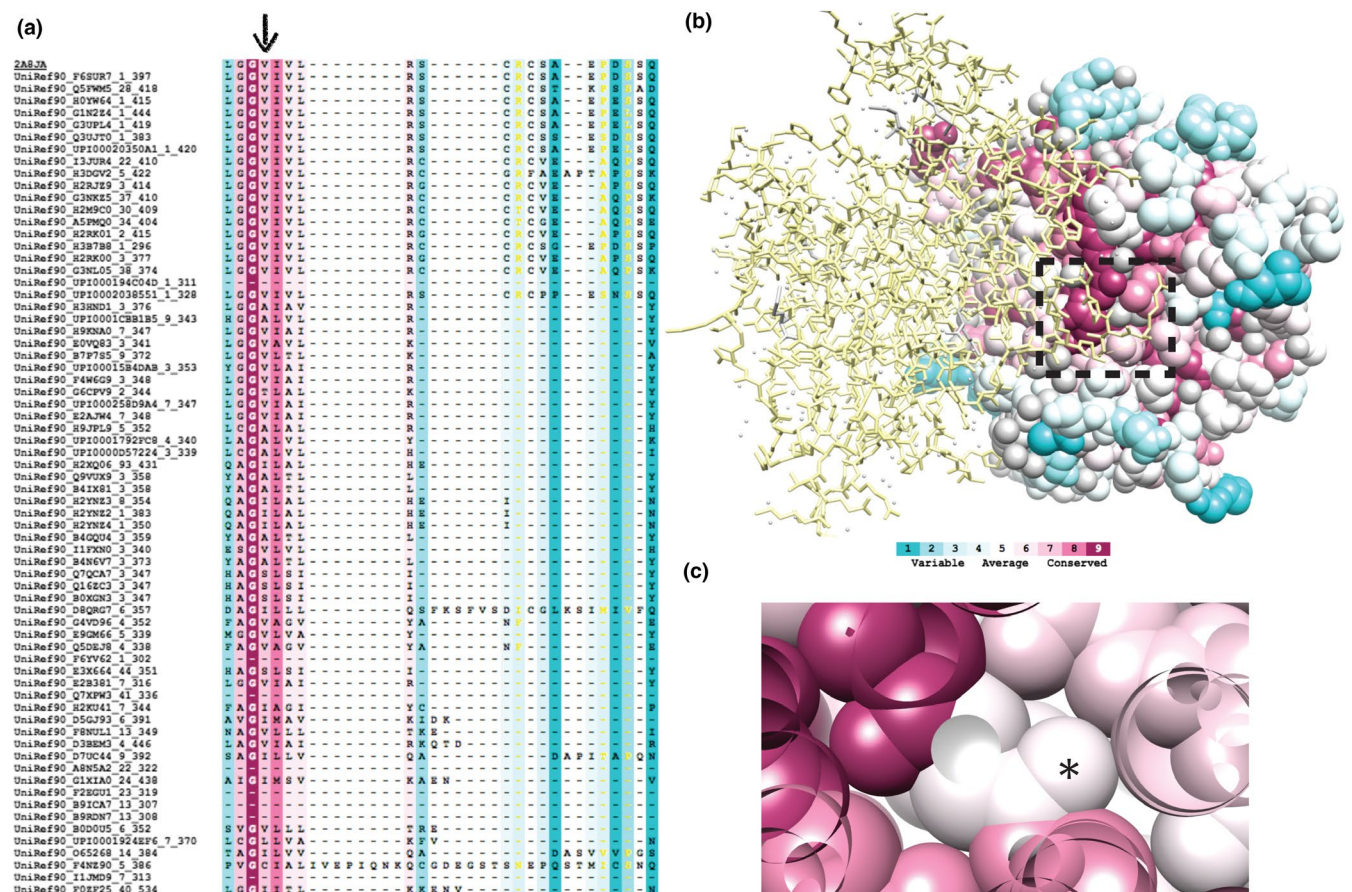


FIGURE 4 Analysis of p.Val343Met Mutation. Amino acid sequence alignment across various species with colors denoting conservation scores (dark pink, highly conserved; dark blue, highly variable) (a, arrow indicates valine 343). Crystal structure of the *TASPI* heterotetramer (b, left, ball and stick representation; right, space filling model color coded to conservation scores, box containing valine 343). Close up view of valine 343 with conservation color analysis (c, star indicates pink valine 343)

ACKNOWLEDGMENTS

The authors thank the family for their participation in this study.

CONFLICT OF INTEREST

None declared.

AUTHOR CONTRIBUTIONS

DMB and MP wrote the manuscript, CMF, MJD, AS and JHP treated the patient and wrote the manuscript.

DATA AVAILABILITY STATEMENT

The data that support the findings of this study are available from the corresponding author upon reasonable request.

ORCID

Daniel M. Balkin  <https://orcid.org/0000-0003-1201-9908>

REFERENCES

- Adzhubei, I. A., Schmidt, S., Peshkin, L., Ramensky, V. E., Gerasimova, A., Bork, P., ... Sunyaev, S. R. (2010). A method and server for predicting damaging missense mutations. *Nature Methods*, 7(4), 248–249. <https://doi.org/10.1038/nmeth0410-248>
- Armstrong, S. A., Staunton, J. E., Silverman, L. B., Pieters, R., den Boer, M. L., Minden, M. D., ... Korsmeyer, S. J. (2002). MLL translocations specify a distinct gene expression profile that distinguishes a unique leukemia. *Nature Genetics*, 30(1), 41–47. <https://doi.org/10.1038/ng765>
- Ayton, P. M., & Cleary, M. L. (2001). Molecular mechanisms of leukemogenesis mediated by MLL fusion proteins. *Oncogene*, 20(40), 5695–5707. <https://doi.org/10.1038/sj.onc.1204639>
- Capotosti, F., Hsieh, J. J., & Herr, W. (2007). Species selectivity of mixed-lineage leukemia/trithorax and HCF proteolytic maturation pathways. *Molecular and Cellular Biology*, 27(20), 7063–7072. <https://doi.org/10.1128/MCB.00769-07>
- Chen, C., Liu, Y. U., Rappaport, A. R., Kitzing, T., Schultz, N., Zhao, Z., ... Lowe, S. W. (2014). MLL3 is a haploinsufficient 7q tumor suppressor in acute myeloid leukemia. *Cancer Cell*, 25(5), 652–665. <https://doi.org/10.1016/j.ccr.2014.03.016>
- Chen, D. Y., Lee, Y., Van Tine, B. A., Searleman, A. C., Westergard, T. D., Liu, H., ... Hsieh, J.-J.-D. (2012). A pharmacologic inhibitor of the protease Taspase1 effectively inhibits breast and brain tumor growth. *Cancer Research*, 72(3), 736–746. <https://doi.org/10.1158/0008-5472.CAN-11-2584>
- Han, S. Y., Zhou, L., Upadhyaya, A., Lee, S. H., Parker, K. L., & DeJong, J. (2001). TFIIAalpha/beta-like factor is encoded by a germ cell-specific gene whose expression is up-regulated with other general transcription factors during spermatogenesis in the mouse. *Biology of Reproduction*, 64(2), 507–517. <https://doi.org/10.1095/biolreprod64.2.507>
- Hoffman, J. D., Ciprero, K. L., Sullivan, K. E., Kaplan, P. B., McDonald-McGinn, D. M., Zackai, E. H., & Ming, J. E. (2005). Immune abnormalities are a frequent manifestation of Kabuki syndrome. *American Journal of Medical Genetics. Part A*, 135(3), 278–281. <https://doi.org/10.1002/ajmg.a.30722>
- Hoiby, T., Zhou, H., Mitsiou, D. J., & Stunnenberg, H. G. (2007). A facelift for the general transcription factor TFIIA. *Biochimica et Biophysica Acta*, 1769(7–8), 429–436. <https://doi.org/10.1016/j.bbexp.2007.04.008>
- Hsieh, J. J., Cheng, E. H., & Korsmeyer, S. J. (2003). Taspase1: A threonine aspartase required for cleavage of MLL and proper HOX gene expression. *Cell*, 115(3), 293–303. [https://doi.org/10.1016/S0092-8674\(03\)00816-X](https://doi.org/10.1016/S0092-8674(03)00816-X)
- Hsieh, J. J., Ernst, P., Erdjument-Bromage, H., Tempst, P., & Korsmeyer, S. J. (2003). Proteolytic cleavage of MLL generates a complex of N- and C-terminal fragments that confers protein stability and subnuclear localization. *Molecular and Cellular Biology*, 23(1), 186–194. <https://doi.org/10.1128/MCB.23.1.186-194.2003>
- Jones, N. C., Lynn, M. L., Gaudenz, K., Sakai, D., Aoto, K., Rey, J.-P., ... Trainor, P. A. (2008). Prevention of the neurocristopathy Treacher Collins syndrome through inhibition of p53 function. *Nature Medicine*, 14(2), 125–133. <https://doi.org/10.1038/nm1725>
- Jones, W. D., Dafou, D., McEntagart, M., Woollard, W. J., Elmslie, F. V., Holder-Espinasse, M., ... Simpson, M. A. (2012). De novo mutations in MLL cause Wiedemann-Steiner syndrome. *American Journal of Human Genetics*, 91(2), 358–364. <https://doi.org/10.1016/j.ajhg.2012.06.008>
- Kang, J. J., Auble, D. T., Ranish, J. A., & Hahn, S. (1995). Analysis of the yeast transcription factor TFIIA: Distinct functional regions and a polymerase II-specific role in basal and activated transcription. *Molecular and Cellular Biology*, 15(3), 1234–1243. <https://doi.org/10.1128/MCB.15.3.1234>
- Khan, J. A., Dunn, B. M., & Tong, L. (2005). Crystal structure of human Taspase1, a crucial protease regulating the function of MLL. *Structure*, 13(10), 1443–1452. <https://doi.org/10.1016/j.str.2005.07.006>
- Kim, D. H., Kim, J., Kwon, J. S., Sandhu, J., Tontonoz, P., Lee, S. K., ... Lee, J. W. (2016). Critical roles of the histone methyltransferase MLL4/KMT2D in murine hepatic steatosis directed by ABL1 and PPARgamma2. *Cell Reports*, 17(6), 1671–1682. <https://doi.org/10.1016/j.celrep.2016.10.023>
- Kim, D.-H., Rhee, J. C., Yeo, S., Shen, R., Lee, S.-K., Lee, J. W., & Lee, S. (2015). Crucial roles of mixed-lineage leukemia 3 and 4 as epigenetic switches of the hepatic circadian clock controlling bile acid homeostasis in mice. *Hepatology*, 61(3), 1012–1023. <https://doi.org/10.1002/hep.27578>
- Kircher, M., Witten, D. M., Jain, P., O’Roak, B. J., Cooper, G. M., & Shendure, J. (2014). A general framework for estimating the relative pathogenicity of human genetic variants. *Nature Genetics*, 46(3), 310–315. <https://doi.org/10.1038/ng.2892>
- Kuo, D. S., Labelle-Dumais, C., & Gould, D. B. (2012). COL4A1 and COL4A2 mutations and disease: Insights into pathogenic mechanisms and potential therapeutic targets. *Human Molecular Genetics*, 21(R1), R97–110. <https://doi.org/10.1093/hmg/dds346>
- Lee, H., Deignan, J. L., Dorrani, N., Strom, S. P., Kantarci, S., Quintero-Rivera, F., ... Nelson, S. F. (2014). Clinical exome sequencing for genetic identification of rare Mendelian disorders. *The Journal of the American Medical Association*, 312(18), 1880–1887. <https://doi.org/10.1001/jama.2014.14604>

- Lee, J., Kim, D.-H., Lee, S., Yang, Q.-H., Lee, D. K., Lee, S.-K., ... Lee, J. W. (2009). A tumor suppressive coactivator complex of p53 containing ASC-2 and histone H3-lysine-4 methyltransferase MLL3 or its paralogue MLL4. *Proceedings of the National Academy of Sciences of the United States of America*, *106*(21), 8513–8518. <https://doi.org/10.1073/pnas.0902873106>
- Lee, J.-E., Wang, C., Xu, S., Cho, Y.-W., Wang, L., Feng, X., ... Ge, K. (2013). H3K4 mono- and di-methyltransferase MLL4 is required for enhancer activation during cell differentiation. *Elife*, *2*, e01503. <https://doi.org/10.7554/eLife.01503>
- Li, X., Yang, Z., Zeng, Y., Xu, H., Li, H., Han, Y., ... You, C. (2013). Cell cycle-related genes p57kip2, Cdk5 and Spin in the pathogenesis of neural tube defects. *Neural Regen Res*, *8*(20), 1863–1871. <https://doi.org/10.3969/j.issn.1673-5374.2013.20.005>
- Matsuo, I., Kuratani, S., Kimura, C., Takeda, N., & Aizawa, S. (1995). Mouse Otx2 functions in the formation and patterning of rostral head. *Genes & Development*, *9*(21), 2646–2658. <https://doi.org/10.1101/gad.9.21.2646>
- Milne, T. A., Briggs, S. D., Brock, H. W., Martin, M. E., Gibbs, D., Allis, C. D., & Hess, J. L. (2002). MLL targets SET domain methyltransferase activity to Hox gene promoters. *Molecular Cell*, *10*(5), 1107–1117. [https://doi.org/10.1016/S1097-2765\(02\)00741-4](https://doi.org/10.1016/S1097-2765(02)00741-4)
- Nakamura, T., Mori, T., Tada, S., Krajewski, W., Rozovskaia, T., Wassell, R., ... Canaani, E. (2002). ALL-1 is a histone methyltransferase that assembles a supercomplex of proteins involved in transcriptional regulation. *Molecular Cell*, *10*(5), 1119–1128. [https://doi.org/10.1016/S1097-2765\(02\)00740-2](https://doi.org/10.1016/S1097-2765(02)00740-2)
- Ng, P. C., & Henikoff, S. (2001). Predicting deleterious amino acid substitutions. *Genome Research*, *11*(5), 863–874. <https://doi.org/10.1101/gr.176601>
- Ng, S. B., Bigham, A. W., Buckingham, K. J., Hannibal, M. C., McMillin, M. J., Gildersleeve, H. I., ... Shendure, J. (2010). Exome sequencing identifies MLL2 mutations as a cause of Kabuki syndrome. *Nature Genetics*, *42*(9), 790–793. <https://doi.org/10.1038/ng.646>
- Niikawa, N., Matsuura, N., Fukushima, Y., Ohsawa, T., & Kajii, T. (1981). Kabuki make-up syndrome: A syndrome of mental retardation, unusual facies, large and protruding ears, and postnatal growth deficiency. *Journal of Pediatrics*, *99*(4), 565–569. [https://doi.org/10.1016/S0022-3476\(81\)80255-7](https://doi.org/10.1016/S0022-3476(81)80255-7)
- Ortega-Molina, A., Boss, I. W., Canela, A., Pan, H., Jiang, Y., Zhao, C., ... Wendel, H.-G. (2015). The histone lysine methyltransferase KMT2D sustains a gene expression program that represses B cell lymphoma development. *Nature Medicine*, *21*(10), 1199–1208. <https://doi.org/10.1038/nm.3943>
- Pomerantz, J., Schreiber-Agus, N., Liégeois, N. J., Silverman, A., Alland, L., Chin, L., ... DePinho, R. A. (1998). The Ink4a tumor suppressor gene product, p19Arf, interacts with MDM2 and neutralizes MDM2's inhibition of p53. *Cell*, *92*(6), 713–723. [https://doi.org/10.1016/S0092-8674\(00\)81400-2](https://doi.org/10.1016/S0092-8674(00)81400-2)
- Prasad, R., Zhadanov, A. B., Sedkov, Y., Bullrich, F., Druck, T., Rallapalli, R., ... Canaani, E. (1997). Structure and expression pattern of human ALR, a novel gene with strong homology to ALL-1 involved in acute leukemia and to Drosophila trithorax. *Oncogene*, *15*(5), 549–560. <https://doi.org/10.1038/sj.onc.1201211>
- Ranish, J. A., Lane, W. S., & Hahn, S. (1992). Isolation of two genes that encode subunits of the yeast transcription factor IIA. *Science*, *255*(5048), 1127–1129. <https://doi.org/10.1126/science.1546313>
- Rao, R. C., & Dou, Y. (2015). Hijacked in cancer: The KMT2 (MLL) family of methyltransferases. *Nature Reviews Cancer*, *15*(6), 334–346. <https://doi.org/10.1038/nrc3929>
- Reva, B., Antipin, Y., & Sander, C. (2011). Predicting the functional impact of protein mutations: Application to cancer genomics. *Nucleic Acids Research*, *39*(17), e118. <https://doi.org/10.1093/nar/gkr407>
- Shawlot, W., & Behringer, R. R. (1995). Requirement for Lim1 in head-organizer function. *Nature*, *374*(6521), 425–430. <https://doi.org/10.1038/374425a0>
- Sherr, C. J. (2001). The INK4a/ARF network in tumour suppression. *Nature Reviews Molecular Cell Biology*, *2*(10), 731–737. <https://doi.org/10.1038/35096061>
- Suleiman, J., Mundt, M., Sampath, S., & El-Hattab, A. W. (2018). TASP1 is deleted in an infant with developmental delay, microcephaly, distinctive facial features, and multiple congenital anomalies. *Clinical Genetics*, *94*(1), 170–173. <https://doi.org/10.1111/cge.13258>
- Takeda, S., Chen, D. Y., Westergard, T. D., Fisher, J. K., Rubens, J. A., Sasagawa, S., ... Hsieh, J. J. (2006). Proteolysis of MLL family proteins is essential for taspase1-orchestrated cell cycle progression. *Genes & Development*, *20*(17), 2397–2409. <https://doi.org/10.1101/gad.1449406>
- Takeda, S., Sasagawa, S., Oyama, T., Searleman, A. C., Westergard, T. D., Cheng, E. H., & Hsieh, J. J. (2015). Taspase1-dependent TFIIA cleavage coordinates head morphogenesis by limiting Cdkn2a locus transcription. *J Clin Invest*, *125*(3), 1203–1214. <https://doi.org/10.1172/JCI77075>
- Tan, S., Hunziker, Y., Sargent, D. F., & Richmond, T. J. (1996). Crystal structure of a yeast TFIIA/TBP/DNA complex. *Nature*, *381*(6578), 127–151.
- Upadhyaya, A. B., Lee, S. H., & DeJong, J. (1999). Identification of a general transcription factor TFIIAalpha/beta homolog selectively expressed in testis. *Journal of Biological Chemistry*, *274*(25), 18040–18048. <https://doi.org/10.1074/jbc.274.25.18040>
- Wang, C., Lee, J.-E., Lai, B., Macfarlan, T. S., Xu, S., Zhuang, L., ... Ge, K. (2016). Enhancer priming by H3K4 methyltransferase MLL4 controls cell fate transition. *Proc Natl Acad Sci U S A*, *113*(42), 11871–11876. <https://doi.org/10.1073/pnas.1606857113>
- Yeoh, E.-J., Ross, M. E., Shurtleff, S. A., Williams, W. K., Patel, D., Mahfouz, R., ... Downing, J. R. (2002). Classification, subtype discovery, and prediction of outcome in pediatric acute lymphoblastic leukemia by gene expression profiling. *Cancer Cell*, *1*(2), 133–143. [https://doi.org/10.1016/S1535-6108\(02\)00032-6](https://doi.org/10.1016/S1535-6108(02)00032-6)
- Zaidi, S., Choi, M., Wakimoto, H., Ma, L., Jiang, J., Overton, J. D., ... Lifton, R. P. (2013). De novo mutations in histone-modifying genes in congenital heart disease. *Nature*, *498*(7453), 220–223. <https://doi.org/10.1038/nature12141>
- Zhou, H., Spicuglia, S., Hsieh, J.-J.-D., Mitsiou, D. J., Hoiby, T., Veenstra, G. J. C., ... Stunnenberg, H. G. (2006). Uncleaved TFIIA is a substrate for taspase 1 and active in transcription. *Molecular and Cellular Biology*, *26*(7), 2728–2735. <https://doi.org/10.1128/MCB.26.7.2728-2735.2006>

How to cite this article: Balkin DM, Poranki M, Forester CM, Dorsey MJ, Slavotinek A, Pomerantz JH. TASP1 mutation in a female with craniofacial anomalies, anterior segment dysgenesis, congenital immunodeficiency and macrocytic anemia. *Mol Genet Genomic Med*. 2019;7:e818. <https://doi.org/10.1002/mgg3.818>